STONE MASONRY CONFINEMENT WITH FRP AND FRCM COMPOSITES

L. Estevan[a], F.J. Baeza[a], D. Bru[a], S. Ivorra[a,*]

[a] Department of Civil Engineering, University of Alicante, P.O. Box 99, 03080 – Alicante, Spain

* Corresponding author sivorra@ua.es

ABSTRACT

In the last decades, there are many reports on the use of composites as reinforcement of structural elements under compression, especially regarding the confinement of concrete structures, but works on stone or masonry columns are limited. Initially, FRP jackets were used because their high structural performance. However, they present some drawbacks like aesthetics or water impermeability, which can affect their applicability in historical constructions made in stone. Recently, FRCM appeared as an alternative with better compatibility with masonry structures. In the present study, a comparison between different composite materials to confine masonry specimens was made. FRPs with carbon or glass fibers and epoxy matrix, and FRCM with basalt or glass fiber mesh in a cementitious matrix were used to confine masonry, made in calcarenite cylindrical pieces and lime mortar. Strength and ductility gains under compressive loads were measured, and compared to the recommendations of different guidelines. Unidirectional FRPs were the optimal solution from a strengthening point of view. On the other hand, FRCM confinement offered more ductility than unreinforced masonry, but showed a softening behavior. Finally, regarding the studied design codes, the specific parameters included for masonry structures seemed enough to obtain accurate predictions of the compressive strength increase due to the confinement with the tested composites.

Keywords: masonry, stone, confinement, FRP, FRCM, TRM.

1. INTRODUCTION

A great deal of the built architectural heritage is made in stone and masonry structural systems. These structures require retrofitting or reinforcement solutions because of the natural degradation of materials, service load changes due to new use, or even to improve the structural response after or in case of extraordinary events, such as fires or earthquakes. In those cases, lateral confinement

could be a suitable solution to gain mechanical strength in columns under longitudinal compression. Traditionally, these reinforcements have been designed using steel profiles. However, composites appeared as an alternative that has been proven successful [1,2]. Composite reinforcements present several advantages, like low self-weight, low maintenance cost and high durability. In addition, they can easily adapt to the external shape of the reinforced element for a less intrusive solution. Nowadays, composites for this type of reinforcement can be classified in two categories depending on the nature of the matrix, polymer or cement. The former, fiber reinforced polymers (FRP) usually use epoxy resins. The latter use modified cement mortars, and are known as fabric reinforced cementitious matrix (FRCM), also identified in scientific literature as textile reinforced mortars (TRM). The use of FRPs in the rehabilitation of civil engineering structures started in the early 1990's [3]. However, in the particular case of heritage constructions, FRCM solutions are recently gaining weight because they present better compatibility with the stone or masonry substrate, and unlike FRP systems based on epoxy resins FRCM layers are permeable coatings in structures with damp or humidity problems [4-6].

Since 1990's, many researchers focused on the effect of FRP jackets to improve the strength of concrete columns [7-11]. These works led to the formulation of different confinement models to simulate the behavior of confined concrete elements with great accuracy [12-14]. On the other hand, FRCM reinforcements have been developed recently, thus there are few reports regarding their use [15-18], and the behavior models are still to be perfectly adapted, especially compared to the confinement with FRP [19]. Nonetheless, most of the research on confinement with either FRCM or FRP has been focused on concrete reinforcement, but some references can be found regarding the effect on masonry or stone elements.

The experimental evaluation of FRP solutions for the confinement of masonry or stone columns has been made considering different sections and ratios, several types of rock, or even with non-continuous reinforcements. Aiello et al. [20,21] studied the confinement of calcareous rock specimens with circular or rectangular cross sections. In these cases, the reinforcement was made in

carbon or glass fiber fabrics (CFRP or GFRP respectively), which were casted as continuous jackets or narrower horizontal stripes with different widths and separations. Continuous FRP jackets increased 93% the strength of the bare masonry, with 200% increase of the ultimate strain. On the other hand, non-continuous confinements may produce the failure of the unreinforced part of the specimen, but if the separation between FRP stripes was limited the performance was similar than a continuous FRP jacket. Faella et al. [22] studied CFRP and GFRP reinforcements, but in specimens from different types of stone (calcareous and volcanic). Both of these confined stones presented a bilinear stress-strain curve, but the transition point between different stiffness changed. In the confinement of the volcanic rock (with lower strength), this transition was detected at the strength of the bare rock, while it appeared at almost twice the strength of calcareous samples. Micelli et al. [23] made a study similar to [20] but, in addition to FRP jackets, including also reinforcements of FRCM or shape memory alloys (in which an active confinement could be achieved). The confinement solutions using FRCM produced a smaller strength gain than FRP alternatives. However, FRCM confinements led to a more ductile behavior, avoiding the brittle failure of the unreinforced masonry. Witzany & Zigler [24,25] tested large scale masonry columns made with regular rectangular stone elements or irregular pieces. In these cases, the confinement was discontinuous and made using horizontal CFRP stripes. A loss of efficiency of the confinement was related to the rectangular cross-section of the specimens or the discontinuous configuration of the confinement. Estevan et al. [26,27] evaluated the effectiveness of CFRP and GFRP continuous jackets in confined rock cylindrical specimens after being exposed to high temperatures inside an oven or using real fire. In these damaged samples, the FRP confinement was capable of achieving strength values similar to undamaged specimens confined with the same material. Regarding the effect of FRCM confinement of masonry elements, few references can be found [28-31]. Finally, the available confinement models for FRP or FRCM jackets and stone or masonry columns are very scarce at the moment and, in fact, are an adaptation of concrete models, in which some parameters have been modified [32,33]. As a summary of these references, in general, the effect of jacketing

with composites on the mechanical performance of masonry specimens has been observed in the increase of their compressive strength (up to three times the strength of unreinforced masonry depending on the properties of the composite), and higher ductility related to the increase of the ultimate strain of the confined masonry. The effectiveness of the confinement may be compromised in elements with rectangular cross section, because the stress concentration in the corners reduces the confinement efficiency, but may be controlled modifying the curvature of the corners. Besides, similar strengthening ratios can be obtained even with discontinuous jackets, in which the distance between consecutive strips should be controlled to obtain an adequate confinement level.

Considering the aforementioned references as a representation of the scientific production in this particular matter (confinement of masonry columns using FRP and FRCM), similar limitations can be found in the recommendations included in the structural design codes of different countries [34-39]. Most of them have considered almost exclusively the confinement of concrete structures. Only the Italian guides, CNR-DT 200 R1/2013 [34] and the recently published CNR-DT 215/2018 [35], make particular considerations for masonry columns and FRP or FRCM confinements, respectively. In both cases, the constitutive laws for confined specimens are analogue to concrete models with slight modifications.

Therefore, the main objective of the current work was aimed at the confinement of cylindrical stone masonry specimens using composite materials (FRP or FRCM jackets). As presented before, there is a lack of references covering this topic, because they are often focused on concrete reinforcement instead of stone or brick masonry. In this case, stone specimens were fabricated with three cylindrical pieces and lime mortar. Afterwards, composite jackets with different fibers and matrices were casted (epoxy resin with carbon or glass fibers, and cement matrix with glass or basalt fiber mesh) to determine the efficacy of each system. In addition, the experimental results have been compared to the predictions based on the recommendations of the Italian guides [34,35], which are the only two that consider specific expressions and coefficients for masonry elements. The stone

samples for this research were calcarenites (San Julian's stone), which was used in the construction of the most important historical buildings in the city of Alicante (Spain).

2. MATERIALS AND METHODS

2.1. Characterization of materials and specimens

The stone samples used in the fabrication of the masonry specimens were obtained from a railway tunnel excavation, under a former quarry near the sea in Alicante (Spain). From the geotechnical survey materials, a total number of 96 calcarenite pieces with cylindrical shape (83 mm diameter and 70 mm high) were selected. Each masonry specimen comprised three of those stone pieces and 4 mm thick mortar joints between them. Therefore, the dimensions of each test specimen were a diameter of 83 mm and a height of 218 mm. The slenderness of the samples, height/diameter ratio, was 2.63, between the recommended values of 2.5 and 3 in the standards for compression tests. In addition, one-piece rock samples with 72 mm diameter and 180 mm height were also prepared in order to characterize the mechanical and physical properties of the rock, according to the procedures in ASTM D7012-14e1 [40]. The average ± standard deviation values of four samples were: bulk density 1982 ± 28 kg/m^3; compressive strength 19.99 ± 1.61 N/mm^2; modulus of elasticity 11859 ± 475 N/mm^2; Poisson's ratio 0.22 ± 0.03. For additional information on the mechanical performance of this rock refer to the following references [41,42]. The lime mortar for the joints was a commercial mixture (53% aggregates and 47% natural lime), with water/binder ratio of 0.60, and a 7.5 N/mm^2 minimum compressive strength after 28 days, according to the supplier. Figure 1 includes an example of the masonry preparation process and the whole set of 32 samples, which were kept in laboratory conditions for 18 months before casting the FRP or FRCM confinement.

Masonry confinement was made with two different types of composite: fiber reinforced polymers (FRP) and fabric reinforced cementitious matrix (FRCM). Three different fabrics were used for the FRP: unidirectional carbon fiber, unidirectional glass fiber and quadraxial glass fiber, as shown respectively in Figure 2 (a), (b) and (c), all of them with an epoxy resin matrix. On the other hand,

FRCM included two different reinforcements, glass fiber mesh (Figure 2(d)) or basalt fiber mesh (Figure 2(e)), and a cement based mortar matrix.

(**a**) (**b**)

Fig. 1. Stone masonry preparation: (a) lime mortar and vertical alignment; (b) 32 masonry specimens before reinforcement.

(**a**) (**b**) (**c**) (**d**) (**e**)

Fig. 2. Fabrics for the FRP reinforcements: (a) unidirectional CFRP; (b) unidirectional GFRP; (c) quadraxial GFRP. Meshes for FRCM jackets: (d) glass fiber mesh; (e) basalt fiber mesh.

The mechanical properties of each composite were measured in direct tensile tests in order to obtain the elastic modulus and tensile strength. Therefore, 15 FRP specimens were prepared, five per each FRP type, in which tensile tests were made according to ASTM D7565/D7565M-10 (2017) [43]. Figure 3 includes the stress-strain results for each sample (CU carbon uniaxial, GU glass uniaxial and GM glass multiaxial); while Table 1 summarizes the mechanical properties for the raw materials (fabrics and resin) according to the supplier, and the composite's properties measured experimentally (average values and coefficient of variation for five samples are given). CFRP samples presented the highest strength and stiffness, 637 MPa and 56 GPa, both calculated with respect to the gross cross section as ASTM D7565 requires [43]. Uniaxial GFRP achieved almost

the same strength level, 539 MPa, because the fabric's weight was higher (900 g/m²). They also showed higher elongation at failure than their CFRP counterparts did, 2.21% against 1.16%. On the other hand, despite the higher fiber dosage of multiaxial fabric (1140 g/m²), these composites presented the lowest mechanical performance because the dimensions and orientation of fibers reduced their efficiency.

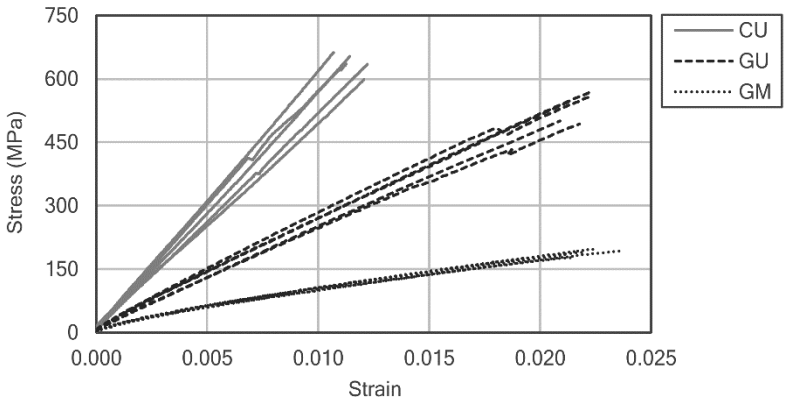

Fig. 3. Stress vs strain results measured in uniaxial tension tests according to ASTM D7565/D7565M-10 (2017) for different FRP types: uniaxial CFRP (CU), uniaxial GFRP (GU), and multiaxial GFRP (GM).

Table 1. Main properties of FRP raw materials and composite specimens.

	Fabric [1]			Epoxy resin [1]	Composite [2]		
	CU	GU	GM		CU	GU	GM
Weight (g/m^2)	300	900	1140	-	-	-	-
Thickness (mm)	0.166 [3]	0.480 [3]	0.438 [3]	-	0.81 [4]	1.08 [4]	1.27 [4]
Tensile strength (MPa)	4830	2560	2600	40	637 (6.43%)	539 (7.48%)	184 (5.50%)
Elastic modulus (MPa)	230000	80700	73000	1400	56078 (7.60%)	25344 (6.06%)	8170 (5.12%)
Ultimate strain (%)	2	3 - 4	3.5 - 4	1.8	1.16 (6.01%)	2.21 (5.15%)	2.09 (8.89%)

[1] Values provided by supplier.
[2] Experimental average values from uniaxial tensile tests (coefficient of variation, in brackets).
[3] Dry fabric thickness.
[4] Composite thickness, measured with micrometer.

For the mechanical properties of FRCM, five coupons of each type were fabricated with dimensions 400x100x9 mm (length x width x thickness). Two different meshes, glass and basalt fibers, were used, both in a cement mortar matrix. The mechanical properties of these three materials as given by the supplier have been included in Table 2. In this case, tensile tests were made following the procedure included in AC434 [44]. The experimental configuration can be observed in Figure 4 (a) and (b), in which the elongation was measured with one LVDT. The mechanical behavior of FRCM

was quite different than FRPs, as shown in Figure 4(c). The idealized behavior included in AC434 [44] is modeled as a bilinear function, which is comprised of an initial elastic response until the cement matrix begins to crack, and after this transition point (T) a strengthening phase may appear depending on the mesh properties and stress transmission between fibers and matrix.

Table 2. FRCM mesh and mortar properties, values provided by supplier.

		Mesh		Mortar
		Glass fiber (GG)	Basalt fiber (BG)	
Mesh size (mm)		12.7 x 12.7	6 x 6	-
Weight (g/m^2)		125	250	-
Thickness (mm) [1]		0.024	0.039	-
Load-resistant area (mm^2/m)		23.51	38.91	-
Strength	(kN/m)	30	60	
	(N/mm^2)	1276 [2]	1542 [2]	≥ 28 [3] ≥ 10 [4]
Elastic modulus (N/mm^2)		72000	89000	11000
Ultimate strain (%)		1.8	1.8	-

[1] Equivalent thickness of dry fabric.
[2] Values obtained from tensile strength (kN/m) and load-resistant area.
[3] Compressive strength after 28 days.
[4] Flexural strength after 28 days.

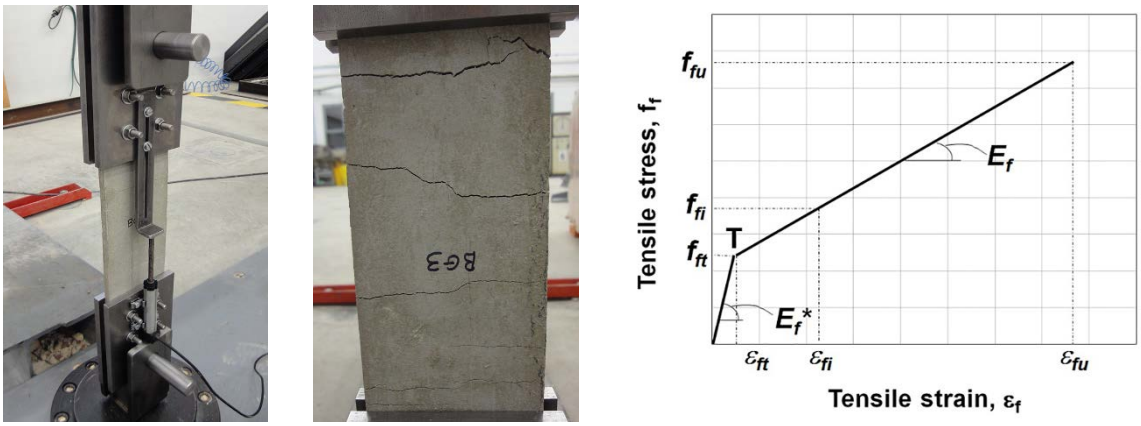

(**a**) (**b**) (**c**)

Fig. 4. Direct tensile test of FRCM specimens: (a) experimental setup; (b) crack pattern of a basalt fiber sample; (c) stress vs strain idealized behavior as shown in AC434.

The mechanical strength depended on the mesh properties, as shown in the experimental results summarized in Figure 5, in which the stress values have been given by fiber's area as AC434 specified [44]. The FRCM responses of each type of fiber were similar to others reported by Leone et al. [45].The mechanical response of FRCM with glass fiber mesh can be observed in Figure 5(a) and did not present the increasing stress-strain behavior after the transition point as shown in the

idealized model of Figure 4(c). Instead, a transition zone appears at a maximum stress of 1200 MPa (approx.), which coincided with the cement matrix cracking, and was very close to the strength of the glass fibers. Afterwards, the progressive failure of each fiber occurred, with different softening curves depending on the actual loading conditions of each particular specimen. On the other hand, basalt fiber FRCM shown in Figure 5(b) presented a bilinear behavior similar to the model in AC434 [44], in which the transition point can be clearly detected and all fibers broke at once. In this case, elongation at failure was almost ten times the elongation corresponding to the transition point. Therefore, the reinforcement effect of the fiber mesh was perfectly registered, unlike glass fiber specimens. Table 3 summarizes all the experimental results of both FRCM according to the indications in AC434 [44], besides the average values of five tested samples, the corresponding coefficient of variation is given in brackets.

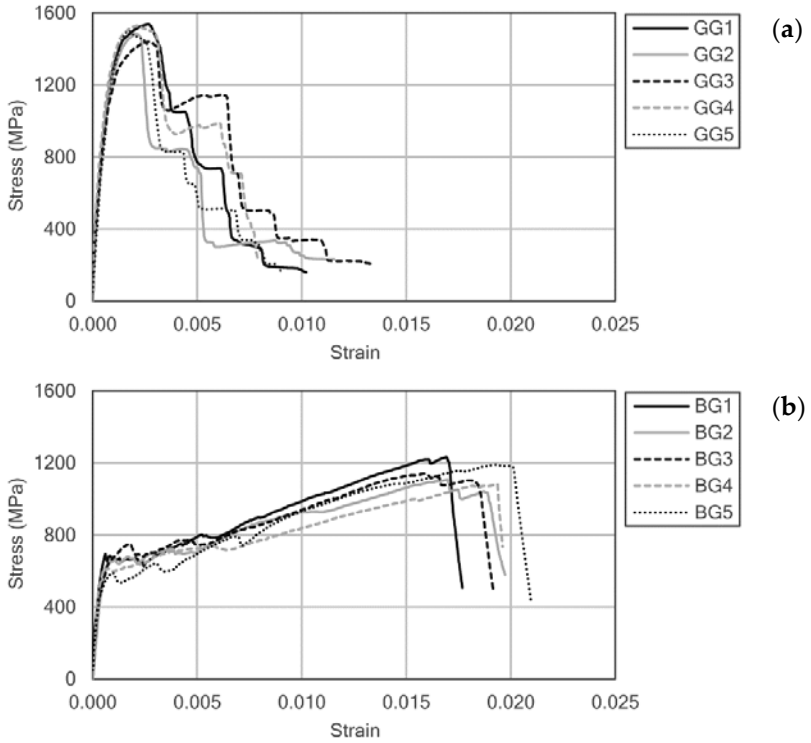

Fig. 5. Tensile test results, stress vs strain of FRCM specimens with (a) glass fiber mesh (GG) or (b) basalt fiber mesh (BG).

Table 3. FRCM properties, experimental values from uniaxial tensile tests [1].

FRCM	f_{ft} (MPa)	ε_{ft}	E_f * (MPa)	f_{fu} (MPa)	ε_{fu}	E_f (MPa)
GG	[2]	[2]	1393 (6.93%)	1474 (4.10%)	0.00273 (13.88%)	[2]
BG	638 (8.20%)	0.00074 (22.35%)	1128 (12.01%)	1177 (6.53%)	0.01771 (8.52%)	38510 (9.30%)

[1] Notation from AC434, Figure 4 (c); coefficient of variation, in brackets.
[2] Unreliable values, according to stress-strain curves.

2.2. Experimental campaign and test setup

Uniaxial compression tests were performed in 32 masonry samples, which have been divided into 8 different sets, each one with a different type of reinforcement, as shown in Table 4. The identification of each sample was made using a six-character code: AA.BB.XX, in which:

- AA referred to the confinement material: N (non-reinforced), CU (uniaxial CFRP), GU (uniaxial GFRP), GM (quadraxial GFRP), GG (glass fiber FRCM) or BG (basalt fiber FRCM).
- BB referred to the number of reinforcement layers: one layer or three layers.
- XX referred to the identification number of the specimens in each set, i.e. 01, 02, 03 or 04.

Figure 6(a) summarizes the FRP reinforcement process, which included: (i) the preparation of the surface with a steel brush and the use of compressed air to remove any loose particles. (ii) Afterwards, the first epoxy layer was brushed all over the lateral surface. (iii) Then the fabric was aligned with the transverse direction of the sample, and to avoid bonding problems a 25% overlap (65 mm) was set. (iv) Finally, lateral pressure to the fabric was applied with an aluminum roller to make the resin flow through the fibers, and the rest of the epoxy was applied at the same time. Once the FRP was casted, samples were kept in laboratory conditions for 7 days to cure at approximately 20°C.

Table 4. Specimen's identification and characteristics of the reinforcement.

Set	Label [1]	Reinforcement	Layers	Samples
01	N.00.XX	-	-	4
02	CU.01.XX	CFRP, uniaxial	1	4
03	GU.01.XX	GFRP, uniaxial	1	4
04	GM.01.XX	GFRP, quadraxial	1	4
05	GG.01.XX	FRCM, glass fiber mesh	1	4
06	GG.03.XX	FRCM, glass fiber mesh	3	4
07	BG.01.XX	FRCM, basalt fiber mesh	1	4
08	BG.03.XX	FRCM, basalt fiber mesh	3	4

[1] 4 samples per set (XX = 01, 02, 03, 04)

On the other hand, the procedure to confine with FRCM was slightly different, as shown in Figures 6(b) and (c). The initial surface treatment was analogue to the one in FRP confined samples (steel brush and compressed air). Before casting the first mortar layer, samples were water-sprayed to avoid that rock specimens absorbed water from the mortar of the FRCM. The FRCM jacket was

casted in three steps: initial mortar layer, 3-4 mm thick; fiber mesh with 50% overlap (130 mm); and second mortar layer 3-4 mm thick. The fresh mortar was finished with a spatula, and in addition, at both ends of the specimen, the mortar was removed in the first 5 mm (Figure 6(c)) in order to avoid direct vertical compression in the jacket during the loading of masonry samples. Finally, samples were kept in laboratory conditions for 28 days. All prepared samples with different reinforcements are shown in Figure 7(a).

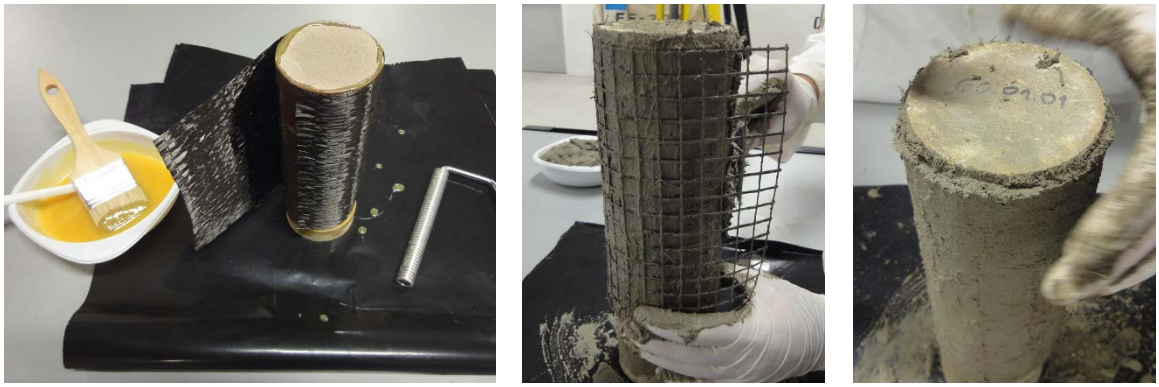

(**a**) (**b**) (**c**)

Fig. 6. Reinforcement of masonry samples with composites: (a) FRP confinement; (b) mortar and fiber mesh of FRCM confinement, and (c) end faces for a proper load application.

(**a**) (**b**)

Fig. 7. Test procedure: (a) general view of the 32 tested samples with different reinforcements; (b) longitudinal compression test setup.

All samples were tested under uniaxial compression in an electromechanical press with a load cell with maximum capacity of 300 kN. Tests were made at a fixed loading rate of 0.5 MPa/s, according to the recommendations in ASTM D7012-14e1 [40]. An example of the experimental setup is shown in Figure 7(b), in which the upper ball and joint guarantees the load alignment, two LVDTs were used to register vertical deformations, and two longitudinal strain gages were attached to the

middle section to monitor transverse strains. A data monitoring device, HBM Spider with Catman software, was used to register all channels at 2 Hz frequency.

3. EXPERIMENTAL RESULTS AND DISCUSSION

Different confinement solutions using FRP and FRCM with several types of fiber, as detailed above, were tested under uniaxial compression to discuss the efficiency of each material in terms of strength increase and ductility. During every test deformations were monitored, longitudinal values were measured using LVDTs, while two strain gages were used in transverse direction. However, in the following discussion only longitudinal strain versus compressive stress curves have been represented for a proper mechanical performance analysis. The transverse strain data have been included only in tables and were used in the analytical study based on different design codes. All the stress-strain curves of masonry specimens below include a thick black curve for the average stress value (4 samples in each set), and a grey-shadowed area corresponding to the 95% bidirectional confidence interval for the stress measure at each strain level. These confidence intervals were calculated according to UNE 66040:2003 [46] and have been only represented in the strain range with at least three measures. In the graphs of confined samples, the average curve corresponding to unreinforced masonry has been also included for a better comparison. During the discussion and analyses, the following notation was used:

f_{mo} Peak compressive strength of unreinforced masonry (MPa)

f_{mc} Peak compressive strength of confined masonry (MPa)

ε_{mo} Strain at failure of unreinforced masonry (longitudinal)

ε_{mc} Strain at failure of confined masonry (longitudinal)

$\varepsilon_{mo,t}$ Strain at failure of unreinforced masonry (transverse)

$\varepsilon_{mc,t}$ Strain at failure of confined masonry (transverse)

ε_{fu} Strain at failure of the FRP or FRCM, obtained in direct tensile tests

g_m Unreinforced masonry mass-density (kg/m³)

E_m Modulus of elasticity of the unreinforced masonry (MPa), determined as the average slope of the straight-line portion of the stress-strain curve [40]

3.1. Unconfined columns

Table 5 includes a summary of the mechanical properties measured in unreinforced masonry specimens. For each property, the average value and the coefficient of variation (in brackets, as percentage) have been included. The compressive strength was similar to other calcarenite specimens (without mortar) tested in other experimental campaign [47]. However, a slight reduction of the elastic modulus was measured, probably because of the lime mortar joints. Figure 8 includes the compressive stress-strain results, and an example of the type of failure of this unreinforced masonry set. The mechanical behavior was linear up to 85% of the material's strength, and failure occurred in a similar way to one-piece calcarenite samples (without lime mortar joints).

Table 5. Unconfined columns: experimental results, average value (coefficient of variation).

f_{mo} (MPa)	ε_{mo}	$\varepsilon_{mo,t}$	E_m (MPa)	g_m (kg/m^3)
20.79 (11.29%)	0.00264 (10.95%)	0.00056 (26.86%)	10973 (14.85%)	2013 (1.79%)

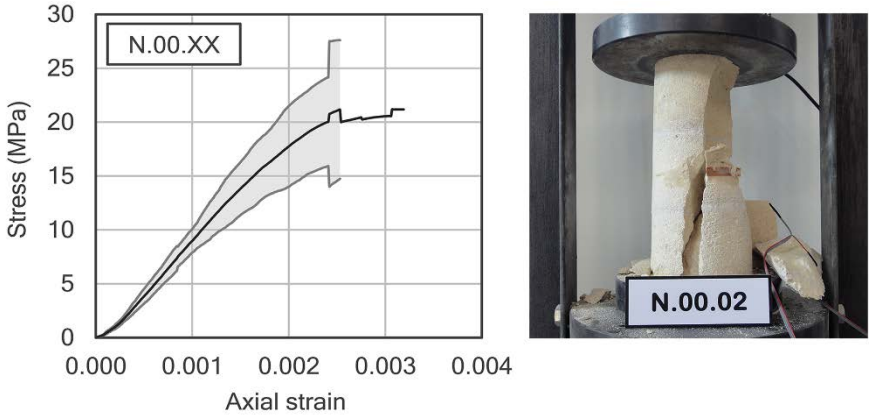

Fig. 8. Unreinforced masonry results: longitudinal stress-strain curve (average ± 95% confidence interval) and failure mode.

3.2. FRP confined columns

The next analysis comprises all samples with FRP reinforcements, with unidirectional glass or carbon fiber or quadraxial glass fiber fabrics. Table 6 summarizes all results of FRP confined

masonry specimens. In addition to the compressive strength or strain at failure values, the ratios between reinforced and unreinforced values (f_{mc}/f_{mo} and $\varepsilon_{mc}/\varepsilon_{mo}$) have also been included to evaluate the effectiveness of the confinement. Transverse ultimate strains (measured with strain gages) have been given in order to evaluate the FRP efficiency factor $k_\varepsilon=\varepsilon_{mc,t}/\varepsilon_{fu}$, as the ratio with respect to the strain at failure of direct tensile FRP samples (included above in Table 1). Actually, this k_ε coefficient represents one of the main differences between the recommendations of different structural codes. Nonetheless, section 4 will include a detailed discussion of the recommendations of the Italian codes CNR-DT 200 R1/2013 [34] and CNR-DT 215/2018 [35].

Table 6. FRP confined masonry: experimental results, average values (coefficient of variation).

Set	f_{mc} (MPa)	f_{mc} / f_{mo}	ε_{mc}	ε_{mc} / ε_{mo}	$\varepsilon_{mc,t}$	ε_{fu}	k_ε
CU.01.XX	41.17 (5.00%)	1.98	0.02217 (26.13%)	8.40	0.00881 (20.82%)	0.0116	0.76
GU.01.XX	39.18 (6.28%)	1.88	0.02864 (16.65%)	10.85	0.01325 (16.11%)	0.0221	0.60
GM.01.XX	31.91 (4.12%)	1.54	0.01904 (10.52%)	7.21	0.00627 (17.68%)	0.0209	0.30

Figure 9 includes the experimental stress-strain curves and failure modes of all three confinements. Both unidirectional laminates, CFRP in Figure 9(a) and GFRP in Figure 9(b), showed the typical bilinear response, which is characteristic of confined concrete or stone elements [8, 20]. The initial elastic response was similar to the unreinforced specimen, as the transverse elongations were too small, and the confinement effect was negligible at this stage. Afterwards, for stresses above the strength of unreinforced masonry, the core started cracking and the second strengthening behavior was registered. The strength increase and especially a high ductility could be easily observed. CFRP led to slightly stronger confinement, while GFRP jackets showed better ultimate strain values for the confined masonry. These results can be related to the mechanical properties of both FRP as shown in Table 1, in which the highest strength was achieved with CFRP laminates, but GFRPs presented an ultimate strain almost twice than CFRP did.

Both unidirectional laminates showed similar failure modes, with explosive failure (due to the brittle behavior of FRP) when the FRP jacket broke in the central section of the masonry specimen. In addition, the damage suffered by the rock core was higher in the CFRP reinforced samples, which broke into smaller stone aggregates.

On the other hand, quadraxial FRP reinforcement didn't show so good results for the experimental conditions of these tests, in which their confinement capacity was limited (there was low fiber weight oriented in transverse direction). Therefore, the strength increase was notably lower than their unidirectional counterparts were, and instead of the strengthening behavior after the transition point, a softening curve was registered, Figure 9(c). On the other hand, the failure mode was more progressive, as the ±45° fibers were capable of controlling it for a non-brittle failure. In these cases, the ultimate strain was determined as the strain corresponding to a stress decrease equal to 20% of the sample's strength [15]. Besides, the core material seemed to be less fractured and disaggregated. Nonetheless, this solution seemed to be the less effective from a confinement point of view, as most of the fibers were not oriented in the best working direction.

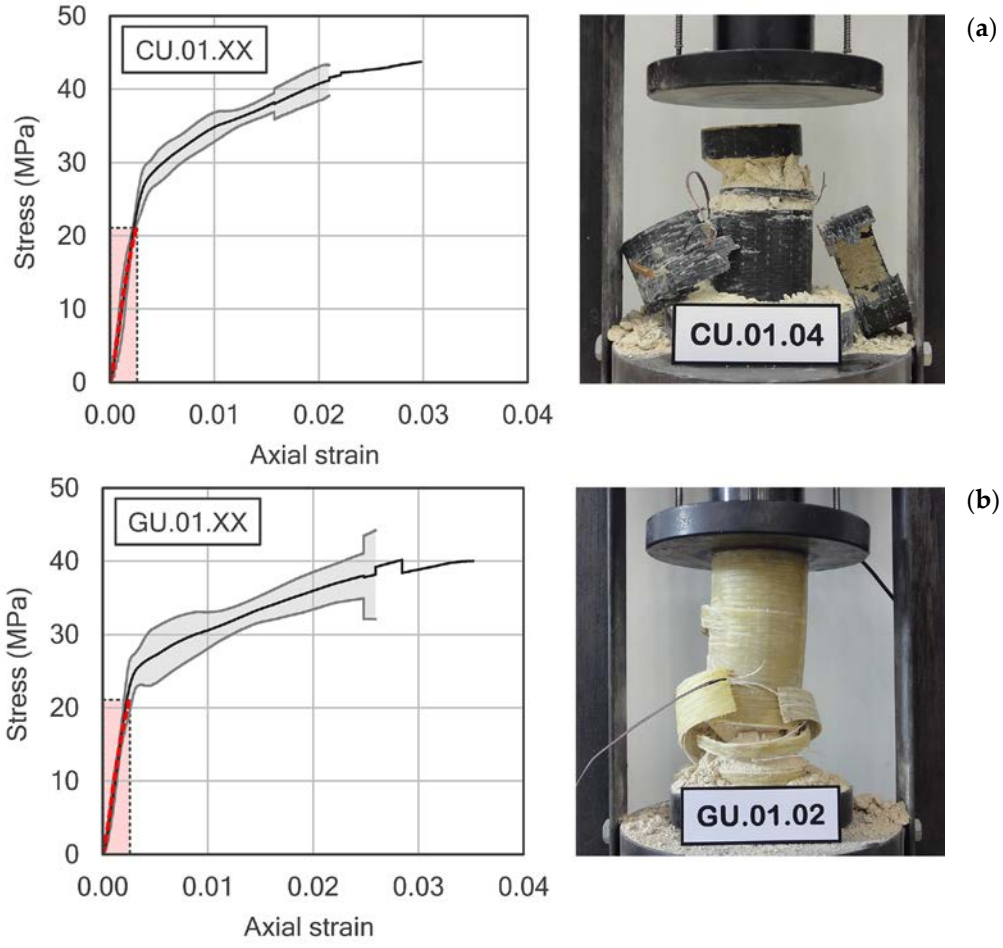

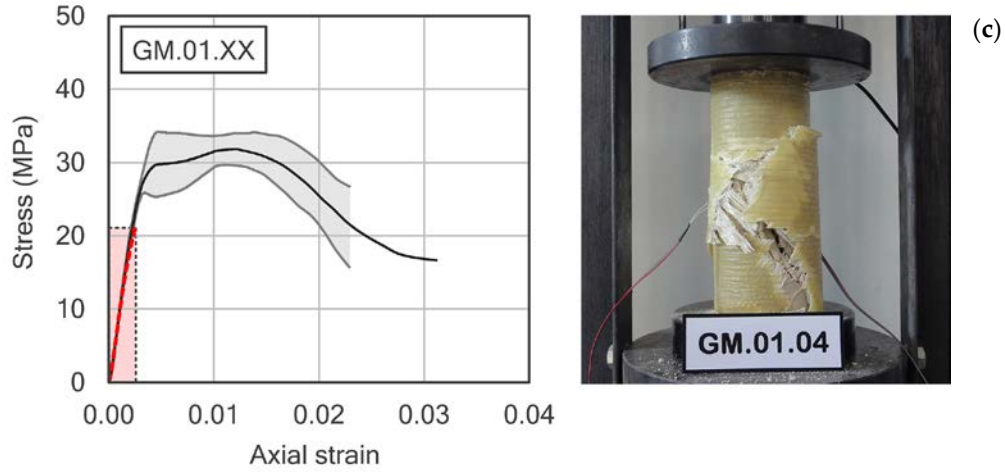

Fig. 9. FRP confined masonry specimens: (a) unidirectional CFRP; (b) unidirectional GFRP; (c) quadraxial GFRP. The average curve of the unreinforced masonry is remarked in the left corner.

3.3. FRCM confined columns

The effect of FRCM confinement in masonry specimens was evaluated using two parameters, the number of layers of the reinforcement mesh (one or three) and the type of fiber (glass or basalt). Table 7 includes a summary of the experimental results, while Figure 10 includes the average stress-strain curves and failure mode of each set.

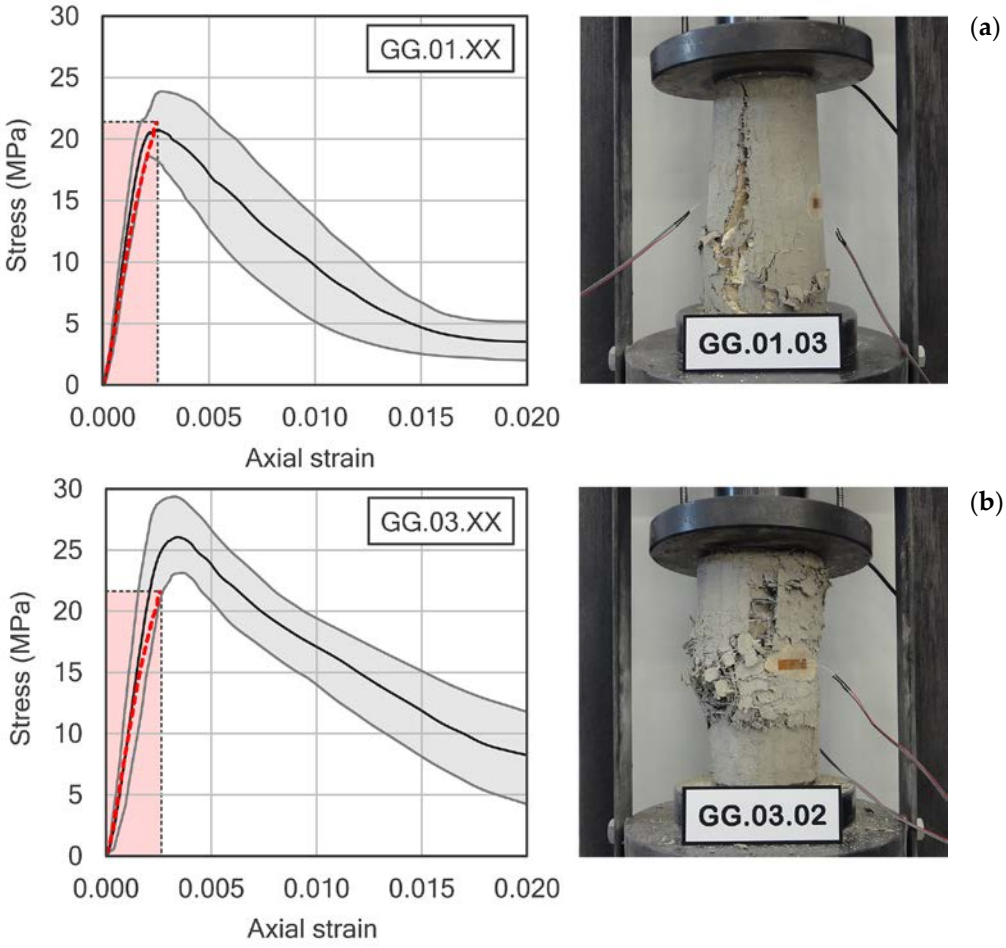

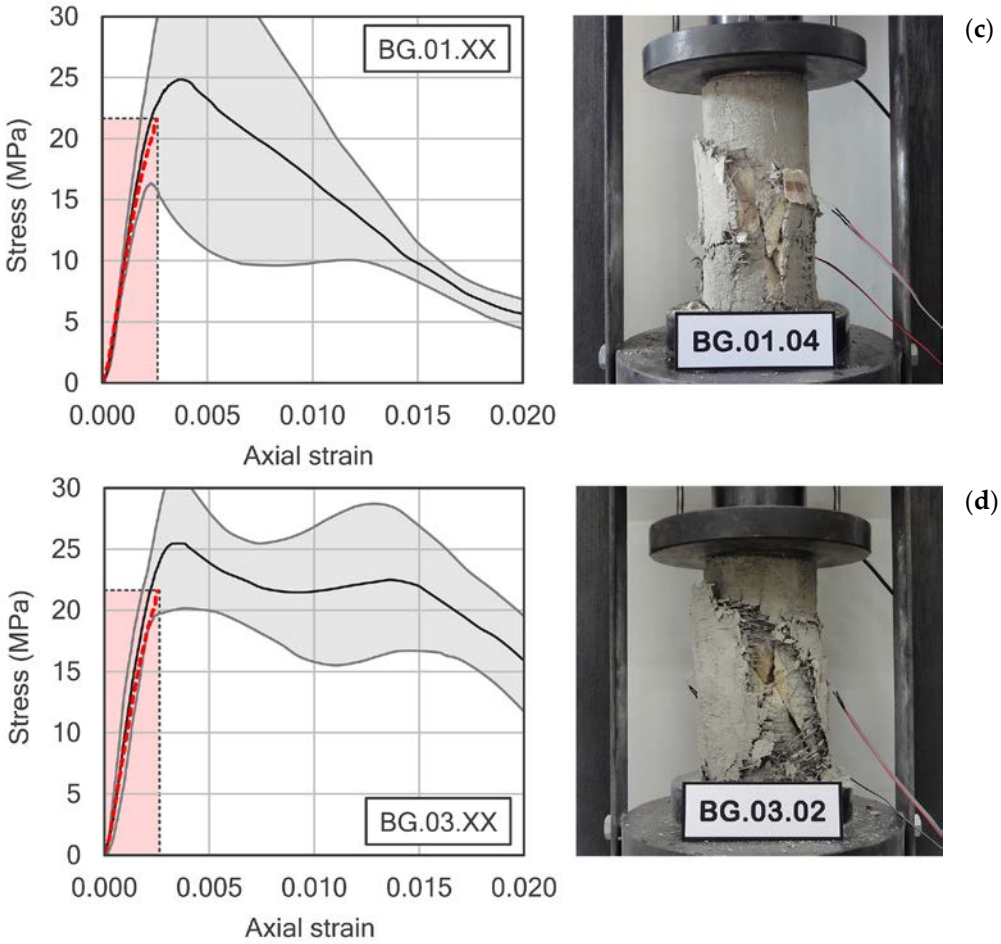

Fig. 10. FRCM confined masonry specimens: (a) 1 layer of glass fiber mesh; (b) 3 layers of glass fiber mesh; (c) 1 layer of basalt fiber mesh; (d) 3 layers of basalt fiber mesh. The average curve of the unreinforced masonry is remarked in the left corner.

In this case, the behavior of FRCM reinforced masonry was different than the aforementioned confinement with FRPs. The dispersion of the results was much bigger in FRCM, e.g. the coefficient of variation for the confined compressive strength was below 6.3% in FRP samples, whilst FRCM confinement presented variations between 6.8% and 26.6%. Basalt fibers showed the most dispersed results, as shown by the confidence intervals in Figure 10. In general, confined samples presented a bilinear response as shown before in FRP confinements, Figure 9(a) and (b), in which after surpassing the strength of the unreinforced rock, the stiffness was reduced but an ascending stress-strain curve was still registered before failure. However, FRCM confinements did not show this hardening behavior, and after the maximum stress, the effect of the jacket was only detected as a ductile behavior capable of controlling the stress loss at higher deformations. At best, FRCM led to a 25% increase of the compressive strength of masonry, when CFRP almost doubled

it. The FRCM with only one layer of glass fiber mesh obtained the same strength level than the bare masonry set. The main difference between mesh types and number of layers was observed in the softening behavior, in which the progressive failure of the reinforcement occurred as fiber meshes broke. Hence, there was not neither an explosive failure nor a clear failure point like those in FRP confined specimens. In order to evaluate the ductility gain, the same criteria explained for FRP confined specimens was used to select failure strain values (20% stress drop after peak stress [15]). These strain values, included in Table 7, the confined samples with better ductility were obtained using basalt fiber meshes. Actually, only the set reinforced with three layers of basalt fibers achieved a deformation level of 1.68% (6 times higher than unreinforced masonry), and similar to FRP confined samples, but with only a 24% strength gain. From the point of view of the failure mode, once again it was completely different to the aforementioned explosive behavior of FRP confinement. As shown in Figure 10, masonry specimens after failure were barely damaged, and the fracture was almost similar to unconfined samples.

Table 7. FRCM confined columns: experimental results, average value (coefficient of variation).

Set	f_{mc} (MPa)	f_{mc} / f_{mo}	ε_{mc}	$\varepsilon_{mc} / \varepsilon_{mo}$	$\varepsilon_{mc,t}$	ε_{fu}	k_{ε}
GG.01.XX	20.95 (9.06%)	1.01	0.00439 (11.32%)	1.66	0.00059 (29.69%)	0.00273	0.22
GG.03.XX	26.22 (6.84%)	1.26	0.00583 (12.19%)	2.21	0.00054 (26.05%)	0.00273	0.20
BG.01.XX	25.09 (26.58%)	1.21	0.00601 (14.06%)	2.28	0.00196 (21.67%)	0.01771	0.11
BG.03.XX	25.74 (11.49%)	1.24	0.01683 (20.20%)	6.37	0.00418 (14.08%)	0.01771	0.23

3.3. Comparative study

Before any further discussion, the differences in the dispersion of results should be remarked. As shown in the confidence intervals of Figures 9 and 10, the behavior of FRP confinements was more homogeneous, and FRCM jackets showed higher dispersion of their mechanical response. For a better comparison between each composite, and their efficiency as confinement solution, Figure 11 includes the strength and strain ratios between reinforced samples and unreinforced masonry, i.e. f_{mc}/f_{mo} and $\varepsilon_{mc}/\varepsilon_{mo}$ respectively. In addition, Figure 11(b) represents the confinement ratios of each system, and Figure 11(c) includes the ratio of the strength gain with respect of the amount of fibers

used in the reinforcement. The strength increase in Figure 11(c) was assessed as (f_{mc}/f_{mo} -1), and the represented ratio considers also the weight of fibers (fabric or mesh) per unit area.

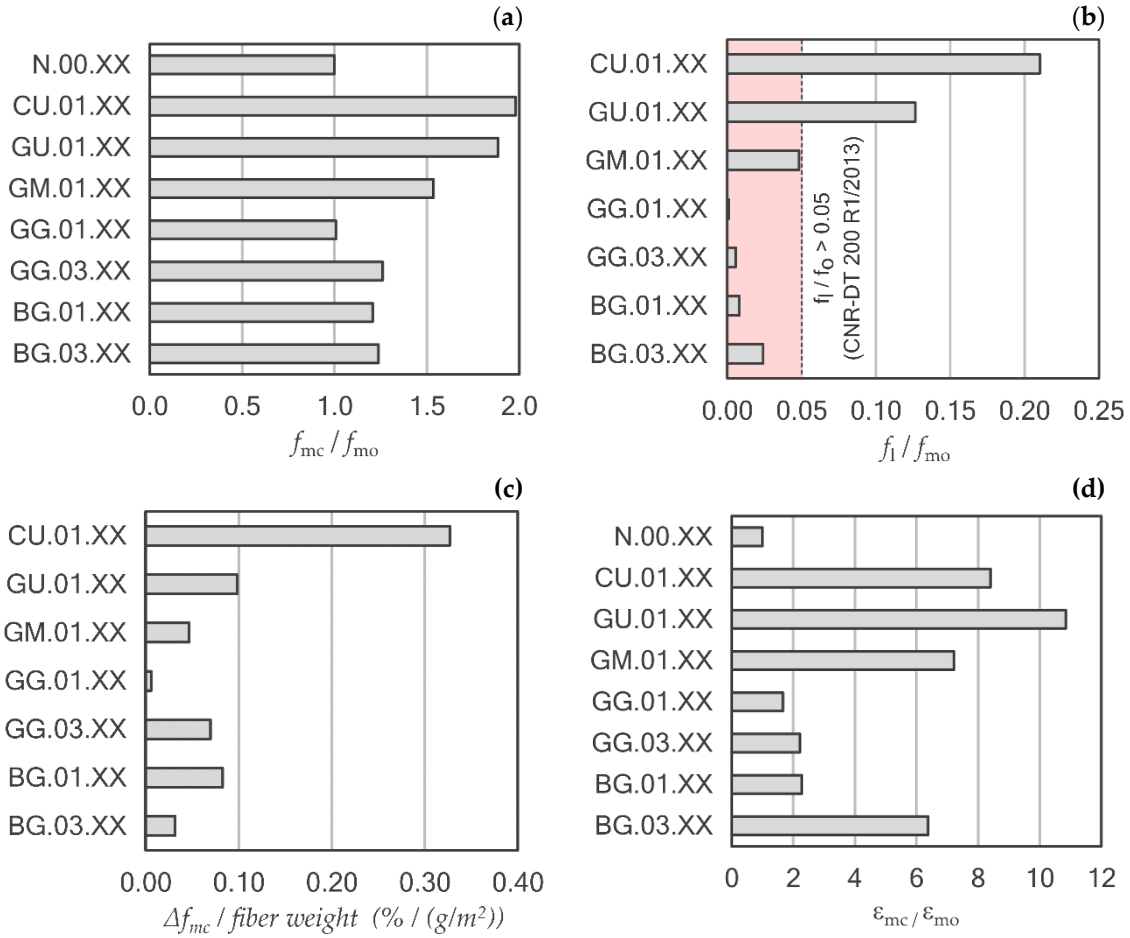

Fig. 11. Confinement efficiency: (a) f_{mc}/f_{mo} ratio; (b) confinement level f_l/f_{mo}; (c) strength increase by fiber weight used for confinement; (d) $\varepsilon_{mc}/\varepsilon_{mo}$ ratio.

If the strength gains are compared, Figure 11(a), CFRP jackets were the most effective solution, whose confinement capacity practically doubled the compressive strength of unreinforced masonry. The uniaxial GFRP achieved almost the same strengthening as CFRP. Despite glass fiber's strength was lower than carbon fibers (Table 1), the GFRP strength was closer to CFRP thanks to a higher fabric weight (GFRP 900 g/m² against CFRP 300 g/m²). Quadraxial glass fiber fabrics only were capable of a 54% strength increase. The effectiveness of each FRP can be also observed in Figure 11(c), in which fabric's weight was also consider. The strength gain was 0.33% (carbon fibers), 0.10% (uniaxial glass fibers) or 0.05% (quadraxial glass fiber) per each unit weight of fiber in the confinement. These results can be justified by the higher mechanical strength of carbon fibers, and the fiber's orientation of quadraxial GFRP.

Nevertheless, FRCM confinements could not achieved these results, and their best mechanical performance (only a 26% improvement) was obtained with three mesh layers. The low mechanical performance can be also explain based on the confinement ratios included in Figure 11(b). Only the confinements made in uniaxial CFRP or GFRP surpass the minimum level of confinement suggested in CNR-DT 200 R1/2013 (f_l/f_{mo}>5%). Hence, based on the actual confinement levels of each material FRCM shouldn't present an increasing stress-strain response [13]. Therefore, the FRCM types tested in this work did not seem as an appropriate solution for the confinement of masonry elements under compression, if a strength increase was expected. However, in other references, a better mechanical performance of these materials was achieved with fibers and mortars with higher mechanical properties, for example, up to three layers of carbon fibers (with strength of 3350 MPa and elastic modulus of 225 GPa) [15], or PBO fibers (strength 5800 MPa, modulus 270 GPa) [18]. In both cases the mechanical properties of the fibers were higher than those used in this research, which can explain the better strengthening result. Nonetheless, this type of FRCM may be a suitable solution for other loading conditions like lateral in-plane loads induced by seismic actions [48].

From the point of view of the increase of the ultimate strain and ductility gain, Figure 11(d), once again unidirectional FRP presented the best results. GFRP jackets increase more than 10 times the ultimate strain of masonry. Confinements with quadraxial fabrics achieved a 7 times strain increase, despite most of the fiber's weight was wasted because their orientation. Finally, according to the current experimental tests the use of FRCM as confinement solution did not seem an appropriate solution. Only several layers of basalt fiber FRCM may have been shown a slight strength increase but with more than six times the ultimate strain (determined for a 20% stress drop after peak stress). Hence, this type of FRCM may be selected to increase the ductility of masonry columns.

3.4. Comparison with design guidelines

In this last section, the experimental results presented above have been compared with the values obtained following the procedure in two Italian guidelines: CNR-DT 200 R1/2013 [34] for FRP strengthening of structures and CNR-DT 215/2018 [35], recently released with specific considerations for FRCM reinforcements. Other available design codes consider confinement models for axially loaded elements [36-39]. In general, the constitutive laws in these codes only include parameters to evaluate concrete structures. Hence, the Italian guidelines were selected because they are currently the only two that considered specific values for masonry or stone structures.

These codes assume a confinement model based on Lam & Teng [13], in which the compressive strength of the confined element (f_{mc}) is related to the unreinforced masonry strength (f_{mo}) according to Eq. (1).

$$f_{mc} = f_{mo}\left[1 + k'\left(\frac{f_{l,eff}}{f_{mo}}\right)^{\alpha_1}\right] \quad (1)$$

where $f_{l,eff}$ is the effective confinement stress; α_1 is a coefficient that can be assumed equal to 0.5, or determined based on experimental tests; k' is a non-dimensional coefficient that can be determined using Eq. (2).

$$k' = \alpha_2\left(\frac{g_m}{1000}\right)^{\alpha_3} \quad (2)$$

where g_m is the unreinforced masonry mass-density (kg/m³) and coefficients α_2 and α_3 may be assumed equal to 1.0, unless additional experimental evidence says otherwise. In addition, the effective confinement stress ($f_{l,eff}$) depends on the shape of the cross section of the confined element, and the material and configuration of the jacket. Both effects are considered in the efficiency factor (k_{eff}), which will be equal to 1.0 in the conditions of the samples in this work (cylindrical samples and continuous jacket, FRP or FRCM, along the total length of each sample). Hence, in the calculations below, the confinement stress f_l matches with the effective confinement stress $f_{l,eff}$.

$$f_{l,eff} = k_{eff} \cdot f_l \approx f_l \quad (3)$$

The lateral confinement stress can be obtained from the equilibrium in a cross section of the confined element, Eq. (4), where n_f is the number of layers in the reinforcement; t_f the thickness of the FRP, or the equivalent thickness of fibers in FRCM reinforcements (without considering the cement matrix); E_f is the elastic modulus of the FRP or the fiber mesh in FRCM; $\varepsilon_{f,red}$ is the reduced strain at failure of the jacket; and D is the diameter of the masonry element to be confined.

$$f_l = \frac{2\, n_f\, t_f\, E_f\, \varepsilon_{f,red}}{D} \tag{4}$$

The reduced strain at failure of the jacket will be obtained differently depending on the type of reinforcement. For example, for FRP confinement the minimum value of two conditions shall be consider, Eq. (5). The first factor includes durability issues: the coefficient η_a depends on the FRP type and the exposure level, for non-exposed elements this factor is 0.95 for CFRP or 0.75 for GFRP; ε_{fu} is the ultimate strain of the FRP in direct tensile tests; finally, γ_f is an additional safety factor equal to 1.10 for confinement reinforcement.

$$\varepsilon_{f,red} = \min\left(\frac{\eta_a \varepsilon_{fu}}{\gamma_f};\, 0.004\right) \tag{5}$$

The second limit, 0.004, is defined to avoid an excessive damage of the masonry core, which could compromise the structural stability, especially under out-of-plane loads. This second condition is also applicable to FRCM reinforcements, Eq. (6), but in that case, the first limit is slightly modified: η_a only depends on the exposure (0.90 in this case) but does not depend on the fiber type of the FRCM. The safety factor γ_m is 1.50 in ULS, and there is and additional non-dimensional factor that considers the matrix characteristics and can be obtained using Eq. (7).

$$\varepsilon_{f,red} = \min\left(\frac{k_{mat}\, \eta_a \varepsilon_{fu}}{\gamma_m};\, 0.004\right) \tag{6}$$

$$k_{mat} = \alpha_4 \left(\frac{4\, t_{mat}}{D} \cdot \frac{f_{c,mat}}{f_{mo}}\right)^2 \leq 1 \tag{7}$$

where α_4 is assumed 1.81 when additional experimental data are unavailable; t_{mat} is the total thickness of the FRCM jacket; and $f_{c,mat}$ is the characteristic compressive strength of the mortar matrix.

Table 8 summarizes the experimental strength values and increases of all tested sets, together with the corresponding predictions obtained with the models in CNR-DT 200 R1/2013 [34] or CNR-DT 215/2018 [35], for FRP or FRCM reinforcements respectively. In the calculations of the guidelines, the parameters α_1, α_2, α_3 and α_4 assumed all aforementioned predefined values. On the other hand, the properties of the reinforcement materials were obtained in tensile tests for the composites (Table 1 and Table 3), and the properties of the raw materials (fibers and cement matrix) were given by the supplier (Table 2). The thickness of the FRPs was measured in the direct tensile samples and assumed the same in the confinement jacket (as the resin dosage was maintained). On the other hand, an average 7 or 10 mm thickness was considered for FRCM jackets with one or three layers. Finally, the strength predictions have been compared to the average experimental capacity, hence the safety factor γ_m in Eq. (6) has been assumed equal to 1.00.

Table 8. Experimental results vs theoretical prediction.

Set	Experimental		Prediction		$f_{mc}^{exp} / f_{mc}^{theo}$	Guide
	f_{mc} (MPa)	f_{mc} / f_{mo}	f_{mc} (MPa)	f_{mc} / f_{mo}		
CU.01.XX	41.17	1.98	39.97	1.92	1.03	CNR-DT 200 R1/2013
GU.01.XX	39.18	1.88	35.66	1.72	1.10	
GM.01.XX	31.91	1.54	29.96	1.44	1.06	
GG.01.XX	20.95	1.01	22.06	1.06	0.95	CNR-DT 215/2018
GG.03.XX	26.22	1.26	23.92	1.15	1.09	
BG.01.XX	25.09	1.21	24.54	1.18	1.02	
BG.03.XX	25.74	1.24	27.30	1.31	0.94	

A comparison between the strength ratios f_{mc}/f_{mo} of the prediction and experimental results has been included in Figure 12. Table 8 included only average values, while all 28 reinforced samples were represented in Figure 12, in which the dispersion of the results could be observed. In general, the dispersion levels were low, only the FRCM with basalt fibers presented more dispersed values, as could be expected with the confidence intervals presented above in Figure 10. The main conclusion of this analysis is the accuracy of the expressions in both guidelines, with errors below 10% that can be acceptable considering the usual dispersion that a material like masonry usually presents.

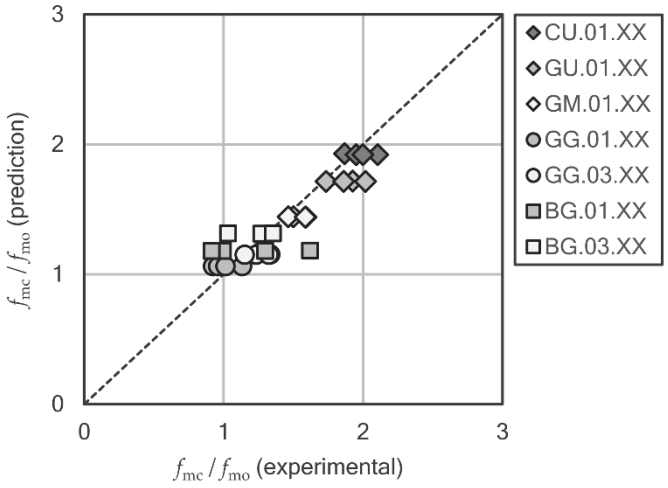

Fig. 12. CNR-DT 200 R1/2013 (FRP) or CNR-DT 215/2018 (FRCM) strength ratios (f_{mc}/f_{mo}) vs experimental results for confined masonry samples.

4. CONCLUSIONS

Masonry samples were prepared using calcarenite pieces from geotechnical surveys and lime mortar. Afterwards, different materials, FRP and FRCM each one with two types of fibers, were used as confinement to test experimentally their reinforcement efficiency. After the tests and different analyses, the following conclusions can be drawn:

1. Masonry samples confined with unidirectional GFRP and CFRP almost doubled the compressive strength of unreinforced masonry. These specimens also showed higher ductility with ultimate strain values up to ten times bigger than unreinforced samples.
2. Quadraxial GFRP presented a limited capacity as confinement solution because fiber orientation. However, the failure mode was more ductile, compared to the explosive brittle failure showed by the other GFRP and CFRP specimens.
3. FRCM jackets presented limited confinement ratio, hence the strength gain was up to 26% of the strength of unreinforced masonry. On the other hand, the stress-strain curves of the confined masonry with FRCM showed a softening behavior (decreasing curves), in which basalt fiber meshes seemed to generate more ductile failures. Higher fiber dosages or fibers with higher strength would be necessary to obtain increasing strain-stress curves with better strength gains.

4. These experimental results were compared with the confinement model predictions of two Italian design guidelines, CNR-DT 200 R1/2013 for FRP and CNR-DT 215/2018 for FRCM. Among all the available codes, these two were selected as the only ones that considered specific values for masonry structures, which led to particularly accurate results, with errors below 10% between the predicted and experimental values.

ACKNOWLEDGMENTS

The authors would like to acknowledge Mapei Spain S.A. for the materials supplied in this research. This research and the APC were funded by Spanish Ministry of Economy and Competitiveness, grant number BIA2015-69952-R and Spanish Ministry of Science, Innovation and Universities, grant number RTI2018-101148-B-I00.

DATA AVAILABILITY

Data may be available upon request to the corresponding author.

REFERENCES

1. S. Ivorra, R. Irles, L. Estevan, J.M. Adam, F.J. Pallarés, B. Ferrer, Drucker-Prager yield criterion application to study the behavior of CFRP confined concrete under compression, 37th IAHS World Congress on Housing, Santander, Spain (2010).
2. D. Bru, S. Ivorra, F.J. Baeza, Seismic behavior of a masonry chimney retrofitted with composite materials: A preliminary approach, Int. J. Saf. Secur. Eng. 7 (2017) 486–497.
3. L.C. Hollaway, A review of the present and future utilisation of FRP composites in the civil infrastructure with reference to their important in-service properties, Constr. Build. Mater. 24 (2010) 2419–2445.
4. S.A. Babatunde, Review of strengthening techniques for masonry using fiber reinforced polymers, Compos. Struct. 161 (2017) 246–255.
5. L.A.S. Kouris, T.C. Triantafillou, State-of-the-art on strengthening of masonry structures with textile reinforced mortar (TRM), Constr. Build. Mater. 188 (2018) 1221–1233.
6. T. Krevaikas D., Experimental study on carbon fiber textile reinforced mortar system as a means for confinement of masonry columns, Constr. Build. Mater. 208 (2019) 723–733.
7. A. Nanni, N.M. Bradford, FRP jacketed concrete under uniaxial compression, Constr. Build. Mater. 9 (1995) 115–124.
8. A. Mirmiran, M. Shahawy, Behavior of concrete columns confined by fiber composites, J. Struct. Eng. (1997) 583–590.
9. H.A. Toutanji, Stress-strain characteristics of concrete columns externally confined with advance fiber composite sheets, ACI Mater. J. 96 (1999) 397–404.
10. S. Pessiki, K.A. Harries, J.T. Kestner, R. Sause, J.M. Ricles, Axial behavior of reinforced concrete columns confined with FRP jackets, J. Compos. Constr. 5 (2001) 237–245.
11. L.-M. Wang, Y.-F Wu, Effect of corner radius on the performance of CFRP-confined square concrete columns: Test, Eng. Struct. 30 (2008) 493–505.
12. M.R. Spoelstra, G. Monti, FRP-confined concrete model, J. Compos. Constr. 3 (1999) 143–150.

13. L. Lam, J.G. Teng, Design-oriented stress–strain model for FRP-confined concrete, Constr. Build. Mater. 17 (2003) 471–489.
14. T. Ozbakkaloglu, J.C. Lim, T. Vincent, FRP-confined concrete in circular sections: Review and assessment of stress–strain models, Eng. Struct. 49 (2013) 1068–1088.
15. T.C. Triantafillou, C.G. Papanicolaou, P. Zissimopoulos, T. Laourdekis, Concrete confinement with textile-reinforced mortar jackets, ACI Struct. J. 103 (2006) 28–37.
16. M. Di Ludovico, A. Prota, G. Manfredi, Structural upgrade using basalt fibers for concrete confinement, J. Compos. Constr. 14 (2010) 541–552.
17. F.J. De Caso y Basalo, F. Matta, A. Nanni, Fiber reinforced cement-based composite system for concrete confinement, Constr. Build. Mater. 32 (2012) 55–65.
18. P. Colajanni, F. De Domenico, A. Recupero, N. Spinella, Concrete columns confined with fibre reinforced cementitious mortars: Experimentation and modelling, Constr. Build. Mater. 52 (2014) 375–384.
19. A. Cascardi, F. Longo, F. Micelli, M.A. Aiello, Compressive strength of confined column with Fiber Reinforced Mortar (FRM): New design-oriented-models, Constr. Build. Mater. 156 (2017) 387–401.
20. M.A. Aiello, F. Micelli, L. Valente, Structural upgrading of masonry columns by using composite reinforcements, J. Compos. Constr. 11 (2007) 650–658.
21. M.A. Aiello, F. Micelli, L. Valente, FRP confinement of square masonry columns, J. Compos. Constr. 13 (2009) 148–158.
22. C. Faella, E. Martinelli, S. Paciello, G. Camorani, M.A. Aiello, F. Micelli, E. Nigro, Masonry columns confined by composite materials: Experimental investigation, Compos. Part B Eng. 42 (2011) 692–704.
23. F. Micelli, R. Angiuli, P. Corvaglia, M.A. Aiello, Passive and SMA-activated confinement of circular masonry columns with basalt and glass fibers composites, Compos. Part B Eng. 67 (2014) 348–362.
24. J. Witzany, R. Zigler, Failure mechanism of compressed reinforced and non-reinforced stone columns, Mater. Struct. 48 (2015) 1603–1613.
25. J. Witzany, R. Zigler, Stress state analysis and failure mechanisms of masonry columns reinforced with FRP under concentric compressive load, Polym. 8 (2016) 176.
26. L. Estevan, F.J. Baeza, V. Brotons, S. Ivorra, FRP confinement of stone specimens after high temperature exposure: Experimental tests, REHABEND, Burgos, Spain (2016) 1457-1464.
27. L. Estevan, F.J. Baeza, S. Ivorra, FRP confinement of fire-damaged calcarenite samples, CMMoST 2017, Madrid, Spain (2017) 317–327.
28. P.E. Mezrea, I.A. Yilmaz, M. Ispir, E. Binbir, I.E. Bal, A. Ilki, External jacketing of unreinforced historical masonry piers with open-grid basalt-reinforced mortar, J. Compos. Constr. 21 (2017) 04016110.
29. A. Cascardi, F. Micelli, M.A. Aiello, FRCM-confined masonry columns: experimental investigation on the effect of the inorganic matrix properties, Constr. Build. Mater. 186 (2018) 811–825.
30. T. Krevaikas D., Experimental study on carbon fiber textile reinforced mortar system as a means for confinement of masonry columns, Constr. Build. Mater. 208 (2019) 723–733.
31. F.S. Murgo, C. Mazzotti, Masonry columns strengthened with FRCM system: Numerical and experimental evaluation, Constr. Build. Mater. 202 (2019) 208–222.
32. G.P. Lignola, R. Angiuli, A. Prota, M.A. Aiello, FRP confinement of masonry: analytical modeling, Mater. Struct. Constr. 47 (2014) 2101–2115.
33. G. Minafò, J. D'Anna, C. Cucchiara, A. Monaco, L. La Mendola, Analytical stress-strain law of FRP confined masonry in compression: Literature review and design provisions, Compos. Part B Eng. 115 (2017) 160–169.
34. CNR-DT 200 R1/2013, Guide for the design and construction of externally bonded FRP systems for strengthening existing structures, National Research Council, Roma, Italy (2014).

35. CNR-DT 215/2018, Istruzioni per la progettazione, l'esecuzione ed il controllo di interventi di consolidamento statico mediante l'utilizzo di compositi fibrorinforzati a matrice inorganica, National Research Council, Roma, Italy (2019).
36. ACI 440.2R-17, Guide for the design and construction of externally bonded FRP systems for strengthening concrete structures, American Concrete Institute, ACI Committee 440 (2017).
37. ACI 549.4R-13, Guide to design and construction of externally bonded fabric-reinforced cementitious matrix (FRCM) systems for repair and strengthening concrete and masonry structures, American Concrete Institute, ACI Committee 549 (2013).
38. TR-55, The Concrete Society Technical Report 55: Design guidance for strengthening concrete structures using fibre composite materials, 3rd Ed., The Concrete Society (2013).
39. FIB Bulletin Nº 14, Externally bonded FRP reinforcement for RC structures, Fédération Internationale du Béton (2001).
40. ASTM D7012-14e1, Standard test methods for compressive strength and elastic moduli of intact rock core specimens under varying states of stress and temperatures, ASTM International, West Conshohocken, PA (2014).
41. V. Brotóns, R. Tomás, S. Ivorra, J.C. Alarcón, Temperature influence on the physical and mechanical properties of a porous rock: San Julian's calcarenite, Eng. Geol. 167 (2013) 117–127.
42. V. Brotons, R. Tomás, S. Ivorra, A. Grediaga, Relationship between static and dynamic elastic modulus of calcarenite heated at different temperatures: The San Julián's stone, Bull. Eng. Geol. Environ. 73 (2014) 791–799.
43. ASTM D7565 / D7565M-10 (2017), Standard test method for determining tensile properties of fiber reinforced polymer matrix composites used for strengthening of civil structures, ASTM International, West Conshohocken, PA (2017).
44. AC434, Acceptance criteria for masonry and concrete strengthening using fabric-reinforced cementitious matrix (FRCM) composite systems, ICC Evaluation Service (2017).
45. M. Leone, M.A. Aiello, A. Balsamo, F.G. Carozzi, F. Ceroni, M. Corradi, M. Gams, E. Garbin, N. Gattesco, P. Krajewski, C. Mazzotti, D. Oliveira, C. Papanicolaou, G. Ranocchiai, F. Roscini, D. Saenger, Glass fabric reinforced cementitious matrix: Tensile properties and bond performance on masonry substrate, Compos. Part B Eng. 127 (2017) 196-214.
46. UNE 66040:2003, Statistical interpretation of test results. Estimation of the mean. Confidence interval, AENOR, Spanish Association for Standardisation (2004).
47. L. Estevan, F.J. Baeza, F.B. Varona, S. Ivorra, FRP retrofitting of calcarenite samples after high temperature exposure, Compos. Struct. (2019) (under review).
48. S. Ivorra, D. Bru, A. Galvañ, S. Silvestri, C. Apera, D. Foti, TRM reinforcement of masonry specimens for seismic areas, Int. J. Saf. Secur. Eng. 7 (2017) 436–474.

List of Tables:

List of Figures:

617 Fig. 8. Unreinforced masonry results: longitudinal stress-strain curve (average ± 95% confidence
618 interval) and failure mode.
619 Fig. 9. FRP confined masonry specimens: (a) unidirectional CFRP; (b) unidirectional GFRP; (c)
620 quadraxial GFRP. The average curve of the unreinforced masonry is remarked in the left corner.
621 Fig. 10. FRCM confined masonry specimens: (a) 1 layer of glass fiber mesh; (b) 3 layers of glass
622 fiber mesh; (c) 1 layer of basalt fiber mesh; (d) 3 layers of basalt fiber mesh. The average curve of
623 the unreinforced masonry is remarked in the left corner.
624 Fig. 11. Confinement efficiency: (a) f_{mc}/f_{mo} ratio; (b) confinement level f_l/f_{mo}; (c) strength increase
625 by fiber weight used for confinement; (d) $\varepsilon_{mc}/\varepsilon_{mo}$ ratio.
626 Fig. 12. CNR-DT 200 R1/2013 (FRP) or CNR-DT 215/2018 (FRCM) strength ratios (f_{mc}/f_{mo}) vs
627 experimental results for confined masonry samples.